Applied Catalysis B: Environmental 180 (2016) 586–595

Contents lists available at ScienceDirect

Applied Catalysis B: Environmental

journal homepage: www.elsevier.com/locate/apcatb

PdAu-MnO_x nanoparticles supported on amine-functionalized SiO_2 for the room temperature dehydrogenation of formic acid in the absence of additives

Yasar Karatas[a], Ahmet Bulut[a], Mehmet Yurderi[a], Ilknur Efecan Ertas[a], Orhan Alal[b], Mehmet Gulcan[a], Metin Celebi[a], Hilal Kivrak[b], Murat Kaya[c], Mehmet Zahmakiran[a,*]

[a] Nanomaterials and Catalysis (NanoMatCat) Research Laboratory, Department of Chemistry, Yüzüncü Yıl University, 65080, Van, Turkey
[b] Department of Chemical Engineering, Yüzüncü Yıl University, 65080, Van, Turkey
[c] Department of Chemical Engineering and Applied Chemistry, Atilim University, 06836, Ankara, Turkey

ARTICLE INFO

Article history:
Received 4 May 2015
Received in revised form 19 June 2015
Accepted 29 June 2015
Available online 17 July 2015

Keywords:
Formic Acid
Hydrogen
Palladium
Gold
Manganese

ABSTRACT

Formic acid (HCOOH) has recently been suggested as a promising hydrogen carrier for fuel cell applications. However efficient hydrogen production through the decomposition of formic acid in the absence of additives under mild thermodynamic conditions constitutes a major challenge because of the ease poisoning of active metals with CO formed as intermediate during formic acid decomposition. Recently, we have reported (App. Catal. B: Env. 164 (2015) 324) our discovery that the separately nucleated MnO_x nanoparticles act as CO-sponge around catalytically active Pd nanoparticles exist on the same support and enhances both the activity and CO-resistivity of Pd nanoparticles. Using this important finding, herein, we present a new catalyst system consists of the physical mixture of PdAu alloy and MnO_x nanoparticles supported on amine-grafted silica (PdAu-MnO_x/N-SiO_2) for the room temperature dehydrogenation of formic acid in the absence of any additives. PdAu-MnO_x/N-SiO_2 catalyst was simply prepared by deposition–reduction technique in water at room temperature with high reproducibility and characterized by the combination of various spectroscopic tools including ICP-OES, P-XRD, DR/UV–vis, XPS, BFTEM, STEM-EDX, STEM-line analysis and CO-stripping voltammetry techniques. The sum of their results shows that the formation of physical mixture of PdAu alloy and MnO_x ($d$mean = 2.2 nm) nanoparticles on the surface of support material. This new catalytic material facilitates the hydrogen liberation through the additive-free formic acid dehydrogenation at room temperature with previously unprecedented activity (TOF = 785 mol H_2 mol catalyst^{-1} h^{-1}), converging to that of the existing state of the art homogenous catalysts. This new superior catalytic system enables facile catalyst recovery and very high stability against agglomeration, leaching and CO poisoning, which make it highly reusable catalyst (retains >92% activity and 85% conversion at the 5th catalytic reuse) in the additive-free formic acid dehydrogenation at room temperature.

1. Introduction

Concerns about the depletion of fossil fuels and global warming motivate the development of more sustainable solutions for the energy problem. In this context, the use of hydrogen as an energy carrier [1,2] is believed to play a growing role in our future society as it can be converted efficiently for the production of electricity and only water is the byproduct when it is utilized in proton exchange membrane fuel cells (PEMFC) [3,4]. However, the safe and efficient storage/release of hydrogen are still among the most important problems faced by the hydrogen economy [1–4]. Hereof, formic acid (HCOOH, FA), which is a liquid at room temperature and contains 4.4% wt hydrogen, is one of the major stable non-toxic products formed in biomass processing and is widely recognized as a potential hydrogen carrier for fuel cells designed towards portable use [5,6]. FA decomposition occurs in the presence of metal catalysts

* Corresponding author at: Department of Chemistry, Yuzuncu Yil University, Campus, Van 65080, Turkey. Fax: +90 432 225 18 06.
E-mail address: zmehmet@yyu.edu.tr (M. Zahmakiran).
URL: http://www.nanomatcat.com (M. Zahmakiran).

http://dx.doi.org/10.1016/j.apcatb.2015.06.060
0926-3373/

by two different pathways, through either dehydrogenation (**1**) or dehydration (**2**) [5,6].

$$HCOOH(l) \rightarrow H_2(g) + CO_2(g) \Delta G^{\circ}_{298K} = -35.0\,kJ/mol \quad (1)$$

$$HCOOH(l) \rightarrow H_2O(l) + CO(g) \Delta G^{\circ}_{298K} = -14.9\,kJ/mol \quad (2)$$

The selective dehydrogenation of FA is indispensable for the production of ultrapure H_2, since toxic carbon monoxide (CO) contamination produced by the dehydration pathway significantly reduces the activity of Pt catalysts in PEMFC [7]. Recently, serious efforts have been conducted on the development of active and selective homogeneous catalysts for FA dehydrogenation [8,9]. Albeit prominent catalytic performances have been achieved in some of these catalysts [10–12] the significant challenges associated with the recovery and reusability significantly hinder the practical use of such catalytic systems in on-board applications. In this context, the recent studies focused on the development of solid supported metal nanoparticles catalysts [14–24] exhibiting significant activity under mild conditions with high selectivity and facile catalyst recovery capabilities. In spite of these plentiful former efforts, the majority of these reported heterogeneous catalysts require elevated temperatures and/or the utilization of extra additives (*e.g.*, HCOONa, NR_3, $LiBF_4$ etc.) [24–26], while revealing low activity and reusability performances [14–16,18–20]. The main reason of the low catalytic performances obtained by these catalytic systems is the ease poisoning of active metal centers by CO, which can form as intermediate in both dehydrogenation and dehydration pathways of FA decomposition [5,6]. In this regard, the development of CO-resistive, active, selective and reusable metal nanocatalysts operating at low temperatures in the additive-free dehydrogenation of FA bears an enormous technological importance. Of particular importance, our recent study [22] has, for the first time, showed that the physical mixture (not alloy or core@shell structures) of Pd and MnO_x nanoparticles supported on amine-grafted silica catalyzes the additive-free FA dehydrogenation at 82% conversion and room temperature. Moreover, the control catalysis experiments coupled with spectroscopic and electrochemical studies have led to the following two important insights

(i) MnO_x nanoparticles exist as the physical mixture with Pd nanoparticles on the support material act as CO-sponge around the catalytically active Pd nanoparticles and enhance activity and lifetime of Pd nanoparticles in the additive-free dehydrogenation of FA under mild conditions. Following this our important discovery, Yan et al.'s paper [23], which was published while we have been writing this manuscript, alike reports that the enhancement in the activity of Pd and PdAu nanoparticles supported on ZIF-8-r-GO (zeolitic imidazole framework-reduced graphene oxide) can be achieved by introducing MnO_x nanoparticles to the catalytic system,

(ii) The existence of $-NH_2$ functionalities grafted onto support enhances the activity of active Pd nanoparticles by affecting the FA adsorption/storage process [27] as well as the nucleation and growth of the Pd and MnO_x nanoparticles on the support surface [22]. More recently, this strong interaction between metal nanoparticles and amine group grafted on support material has been named as "Strong Metal-Molecular Support Interaction" (SMMSI) by Yadav et al. [28].

These important insights have encouraged us to use MnO_x/SiO_2-APTS system for the development of new Pd based active and CO-resistive nanocatalysts for additive-free FA dehydrogenation. Along these lines, herein we present a facile synthesis of PdAu alloy and MnO_x nanoparticles (NPs) supported on 3-aminopropyltriethoxysilane functionalized silica, which will hereafter be referred to as PdAu-MnO_x/N-SiO_2, and their superior catalysis for the dehydrogenation of pure FA solution at room temperature. PdAu-MnO_x/N-SiO_2 catalyst was prepared with high reproducibility through (*i*) 3-aminopropyltriethoxysilane (APTS) functionalization of SiO_2, (*ii*) wet-impregnation of metal cations onto APTS-functionalized SiO_2 support and (*iii*) subsequent sodium borohydride ($NaBH_4$) reduction in water all at room temperature [22,29]. The structural characterization of PdAu-MnO_x/N-SiO_2 was performed by using a combination of multi-pronged analytical techniques including inductively coupled plasma-optical emission spectroscopy (ICP-OES), powder X-ray diffraction (XRD), Fourier transform infrared spectroscopy (FTIR), X-ray photoelectron spectroscopy (XPS), diffuse reflectance UV–vis (DR-UV–vis) spectroscopy, bright-field transmission electron microscopy (BFTEM), scanning transmission electron microscopy-energy dispersive X-ray spectroscopy (STEM-EDX), STEM-point analyses and CO-stripping voltammetry technique. These comprehensive structural characterization efforts reveal the presence of well-dispersed and separately nucleated PdAu alloy and MnO_x NPs with a mean diameter of 2.2 nm. The resulting PdAu-MnO_x/N-SiO_2 material can catalyze additive-free FA dehydrogenation with record catalytic activity (turnover frequency (TOF) = 785 mol H_2 mol catalyst^{-1} h^{-1} at >99% conversion) even at room temperature. Moreover, the exceptional durability of PdAu-MnO_x/N-SiO_2 catalyst against agglomeration, leaching and CO poisoning renders this catalytic architecture an excellent contender as a reusable heterogeneous catalyst in the hydrogen production from formic acid for on-board fuel cell applications.

2. Experimental

2.1. Materials

Palladium(II) nitrate dihydrate ($Pd(NO_3)_2{\cdot}2H_2O$), manganese(II) chloride dihydrate ($MnCl_2{\cdot}2H_2O$), gold(III) chloride trihydrate ($AuCl_3{\cdot}2H_2O$), 3-aminopropyltriethoxysilane ($H_2N(CH_2)_3Si(OC_2H_5)_3$, APTS), sodium borohydride ($NaBH_4$), ninhydrin ($C_9H_6O_4$), toluene (C_7H_8) and sodium hydroxide (NaOH) were purchased from Sigma–Aldrich®. Formic acid (CH_2O_2, >96%), and silica gel (230–400 mesh) were purchased from Merck®. Toluene was distilled over sodium and stored in a Labsconco nitrogen-atmosphere drybox (O_2 < 1 ppm). Deionized water was distilled by water purification system (Milli-Q Water Purification System). All glassware and teflon-coated magnetic stirring bars were washed with acetone and copiously rinsed with distilled water before drying in an oven at 423 K.

2.2. Characterization

Pd, Au and Mn contents of the samples were determined by ICP-OES (Leeman, Direct Reading Echelle) after each sample was completely dissolved in a mixture of HNO_3/HCl (1/3 v/v) by gentle heating. Powder X-ray diffraction (XRD) patterns were recorded with a MAC Science MXP 3TZ diffractometer using Cu-Kα radiation (wavelength 1.54 Å, 40 kV, 55 mA). BFTEM, HRTEM and STEM samples were prepared by drop wise addition of the dilute catalyst suspension on a copper-coated carbon TEM grid followed by the evaporation of the solvent. The conventional TEM measurements were carried out on a JEOL JEM-200CX transmission electron microscope operating at 120 kV. HRTEM, STEM and HAADF-STEM analysis were performed using a JEOL JEM-2010F transmission electron microscope operating at 200 kV. Oxford EDX system and the Inca software were exploited to acquire and process STEM-EDX data. The XPS measurements were employed via a Physical Electronics 5800 XP spectrometer equipped with a hemispherical analyzer and a monochromatic Al-Kα X-Ray source (1486.6 eV,

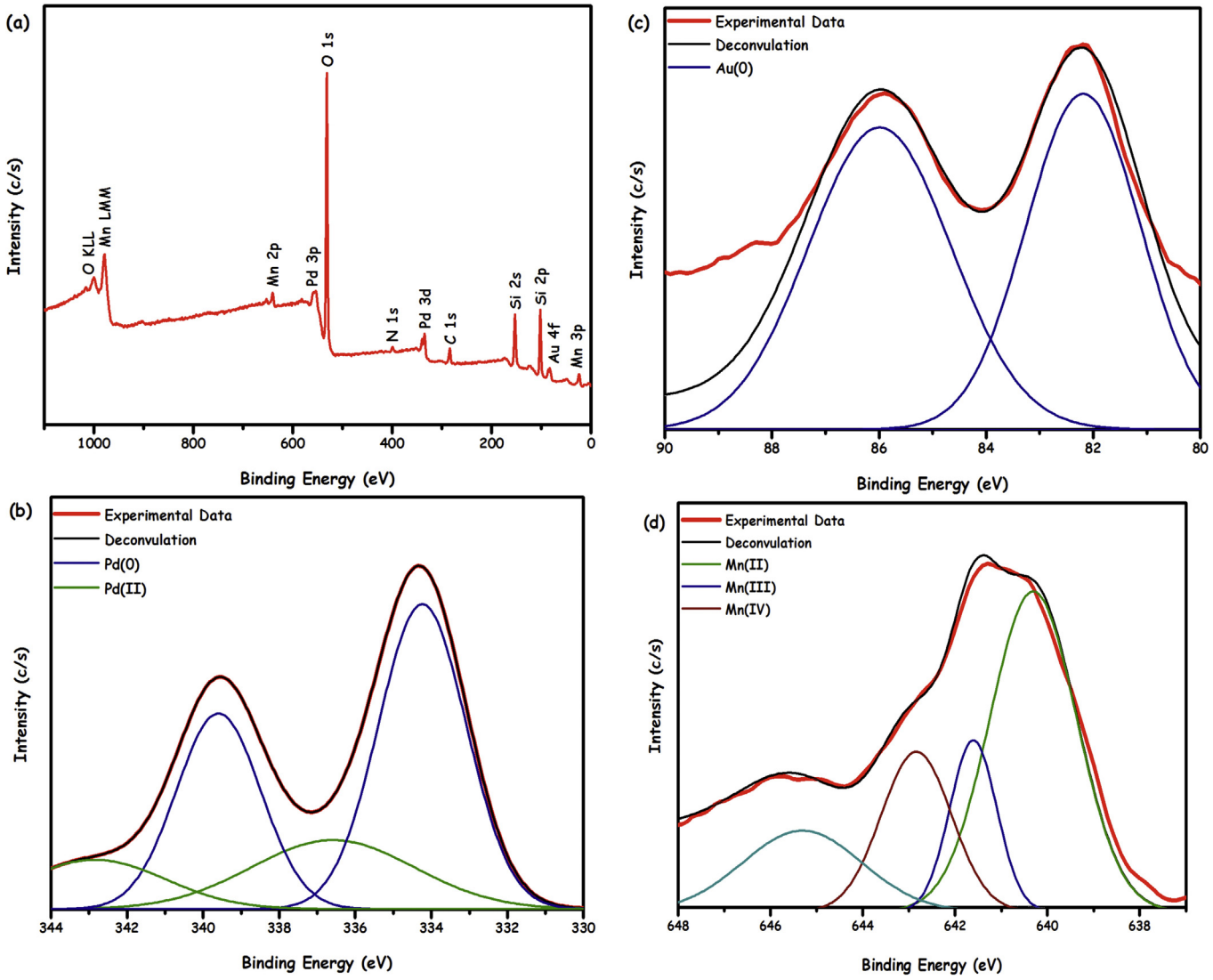

Fig. 1. (a) Survey XPS spectrum, (b) high resolution Pd 3d XPS spectrum, (c) high resolution Au 4f XPS spectrum and (d) high resolution Mn 2p XPS spectrum of PdAu-MnO_x/N-SiO_2 catalyst.

15 kV, 350 W, with pass energy of 23.5 eV). Gas phase decomposition products of formic acid were analyzed by gas chromatography using FID-2014 and TCD-2014GC analyzers (Shimadzu) and FTIR spectroscopy (Shimadzu IR-Affinity). DR/UV–vis and UV–vis spectra were taken by using Shimadzu UV-3600 with integrating sphere attachment.

2.3. Catalyst preparation

The functionalization of the silica was carried out by adding a desired amount of APTS to 30 mL of dry toluene containing 500 mg of silica. The resulting slurry was stirred for 12 h. The white solid was filtered and washed repeatedly with toluene. The white amine-functionalized silica (N-SiO_2) was dried in a vacuum oven (373 K and 10^{-1} Torr) and used for further application. The presence of $-NH_2$ functionalities on the SiO_2 support surface was quantified by the colorimetric ninhydrin method [30]. PdAu-MnO_x/N-SiO_2 catalyst was obtained by the conventional impregnation and subsequent reduction steps [31]. Typically, 5.0 mL aqueous solution containing $Pd(NO_3)\cdot 2H_2O$ (12.35 mg, 46.3 μmol Pd), $AuCl_3\cdot 2H_2O$ (11.4 mg, 28.9 μmol Au), $MnCl_2\cdot 2H_2O$ (3.1 mg, 19.1 μmol Mn) and N-SiO_2 (140 mg, 140 μmol NH_2) is mixed for 3 h. Then, the fresh 1.0 mL aqueous solution of $NaBH_4$ (56 mg, 1.4 mmol) was added to this mixture and the resulting solution was stirred for half an hour under ambient conditions. After centrifugation (6000 rpm, 5 min), copious washing with water (3 × 20 mL), filtration, and drying in oven at 373 K, PdAu-MnO_x/N-SiO_2 catalyst was obtained as a dark gray powder.

2.4. Activity measurements

The catalytic activity of PdAu-MnO_x/N-SiO_2 in the additive-free FA dehydrogenation was determined by volumetric measurement of the rate of hydrogen evolution. The volume of released gas during the reaction was monitored using a gas burette through water displacement as described elsewhere [13–21]. Before starting the catalytic activity tests, a jacketed one-necked reaction flask (50.0 mL) containing a teflon-coated stirring bar was placed on a magnetic stirrer (Heidolph MR-3004) whose temperature was adjusted by circulating water through its jacket from a constant temperature bath (Lab Companion RW-0525). In a typical catalytic activity test, PdAu-MnO_x/N-SiO_2 catalyst was weighed and transferred into the reaction flask, and then 9.0 mL H_2O was added into the reaction flask followed by rigorous stirring for 15 min to achieve

thermal equilibrium. Next, 0.5 mL aqueous FA solution (0.075 mL FA + 0.425 mL H_2O) was added into the reaction flask *via* its septum using a 1.0 mL gastight syringe and the catalytic reaction was started (t = 0 min) by stirring the mixture at 600 rpm.

2.5. Catalytic selectivity

The selectivity of PdAu-MnO_x/N-SiO_2 catalyst in the decomposition of FA was investigated by GC, FTIR analyses and NaOH-trap experiments. The gas generated over PdAu-MnO_x/SiO_2-NH_2 catalyzed dehydrogenation of aqueous FA solution (10.0 mL of 0.2 M) was separately collected in GC analyzing balloon and FTIR gas sample holder, which were then analyzed in GC and FTIR by using pure CO, H_2 and CO_2 as reference gases. NaOH-trap experiments were performed to determine the molar ratio of CO_2 to H_2 in the product mixture generated during the PdAu-MnO_x/SiO_2-NH_2 catalyzed decomposition of aqueous FA solution (10 mL of 0.2 M) [13,21]. In these experiments, the trap (10.0 M NaOH solution) was placed between the jacketed reactor and gas burette. The generated gas during the reaction was passed through the NaOH trap where CO_2 was captured (**3**). Next, the volume of the gas generated from the dehydrogenation of FA was monitored and compared to those without the trap experiment. We observed that the volume of the generated gas decreased by a factor of two in the presence of the NaOH trap. This result is indicative of the complete adsorption of CO_2 in NaOH solution (**3**) and the presence of equivalent molar amounts of CO_2 and H_2 (1.0:1.0) in the product mixture of the PdAu-MnO_x/SiO_2-NH_2 catalyzed additive-free FA dehydrogenation.

$$2NaOH(aq) + CO_2(g) \rightarrow Na_2CO_3(aq) + H_2O(l) \quad (3)$$

2.6. Catalytic stability

The catalyst was isolated from the reaction solution by centrifugation after the first catalytic run and washed with excess water and dried at 373 K. The dried catalyst was weighed and reused in the catalytic dehydrogenation of a 10.0 mL aqueous FA solution (0.075 mL FA + 9.925 mL H_2O) at 298 K. The used catalyst was isolated and reused up to 5 consecutive catalytic cycles.

2.7. CO Stripping voltammetry measurements

CO stripping voltammetry measurements were carried out in a conventional three-electrode cell with a Pt wire as the counter electrode and Ag/AgCl as the reference electrode with a CHI 660E potentiostat. The working electrode was a glassy carbon disk having a diameter of 3.0 mm held in a Teflon cylindrical housing. 5 mg catalyst sample was dispersed in 1.0 mL 5% Nafion® solution (Aldrich) to obtain a catalyst suspension. Next, 5.0 μL of this suspension was drop-cast on the surface of the glassy carbon electrode. All electrolyte solutions were deaerated with high-purity nitrogen for 30 min prior to the measurements. For CO stripping voltammetry, a 0.5 M H_2SO_4 solution was first bubbled with pure nitrogen for 30 min in order to remove the dissolved oxygen. CO was then purged into the solution for 20 min to allow saturation of the electrocatalyst surface with adsorbed CO, while maintaining a constant potential of 0.0 V. Excess CO was then purged with nitrogen for 30 min.

3. Results and discussion

Prior to the preparation of PdAu-MnO_x/N-SiO_2, APTS grafting onto SiO_2 support material was made by refluxing of APTS and activated SiO_2 in dry toluene. The grafting of APTS onto SiO_2 support was evidenced by FTIR spectroscopy and quantified by ninhydrin method (*vice versa*) [30]. The direct comparison of FTIR spectra of SiO_2 (unmodified) and APTS grafted-SiO_2 (Fig. S1) is indicative of the successful post-grafting of APTS onto SiO_2 support, which is confirmed by the appearance of several new peaks in the ranges of 3000–2800 cm^{-1} and 750–650 cm^{-1} due to C—H stretching and N—H bending vibrations of APTS, respectively [32]. Afterwards, PdAu-MnO_x/N-SiO_2 catalyst was simply and reproducibly prepared by following the procedure comprising of the conventional impregnation of Pd(II), Au(III) and Mn(II) onto support and their subsequent $NaBH_4$ reduction in water all at room temperature. After centrifugation, copious washing with water, and drying under vacuum PdAu-MnO_x/N-SiO_2 catalyst was obtained as powders and characterized by the combination of various spectroscopic tools including ICP-OES, P-XRD, DR/UV–vis, XPS, BFTEM, HRTEM, TEM-EDX, STEM-EDX-line analysis and CO-stripping voltammetry techniques.

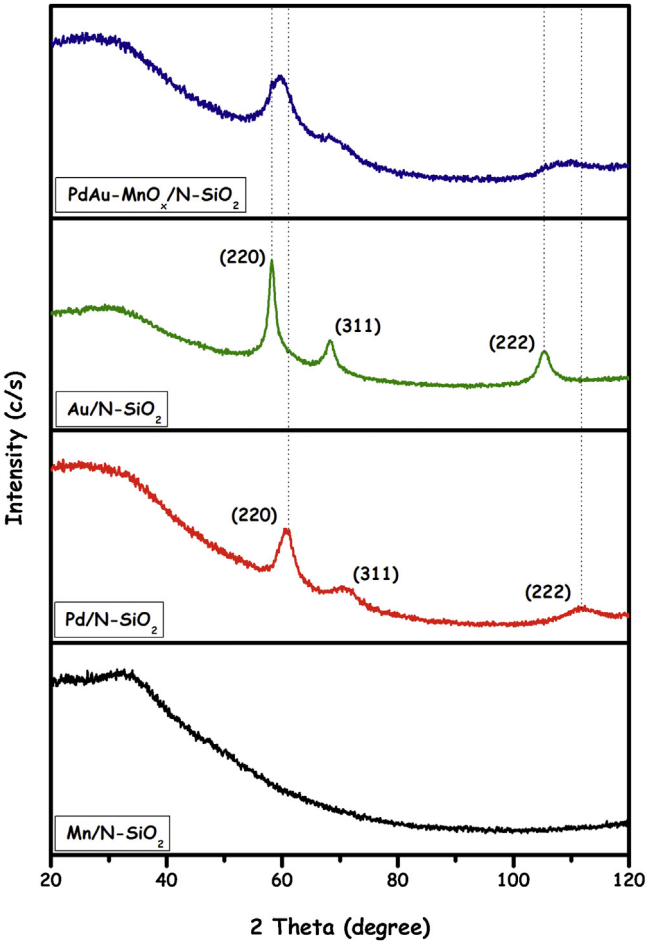

Fig. 2. P-XRD patterns of Mn /N-SiO_2, Pd/N-SiO_2, Au/N-SiO_2 and PdAu-MnO_x/N-SiO_2.

The metals and free amine contents of the as-prepared catalyst were found to be 2.51% wt Pd (35 μmol), 2.79% wt Au (21 μmol), 0.52% wt Mn (14 μmol) (corresponds to $Pd_{0.5}Au_{0.3}Mn_{0.2}$) and 0.98 mmol NH_2/g SiO_2 by ICP-OES analyses and ninhydrin method [30]. The surface composition and the oxidation states of Pd, Au and Mn were investigated by using XPS. Fig. 1(a) shows the survey XPS spectrum of PdAu-MnO_x/N-SiO_2, which depicts the existence of Pd, Au and Mn in addition to the elements of APTS-functionalized SiO_2 support (Si, N, O). The high resolution Pd 3d, Au 4f and Mn 2p XPS spectra of PdAu-MnO_x/N-SiO_2 together with their deconvoluted chemical states are given in Fig. 1(b)–(d). The inspection of Pd 3d and Au 4f spectra reveals the presence of mainly metallic Pd (*i.e.*, Pd^0 with Pd $3d_{5/2}$ at 334.2 eV and Pd $3d_{3/2}$ at 339.6 eV) [33] and

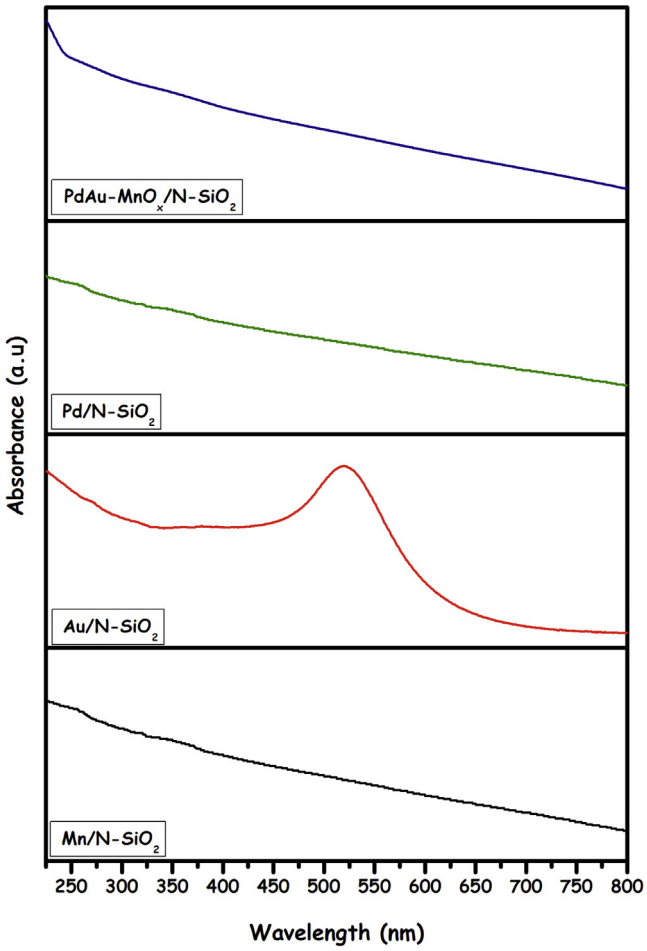

Fig. 3. DR-UV–vis spectra of Mn /N-SiO_2, Pd/N-SiO_2, Au/N-SiO_2 and PdAu-MnO_x/N-SiO_2.

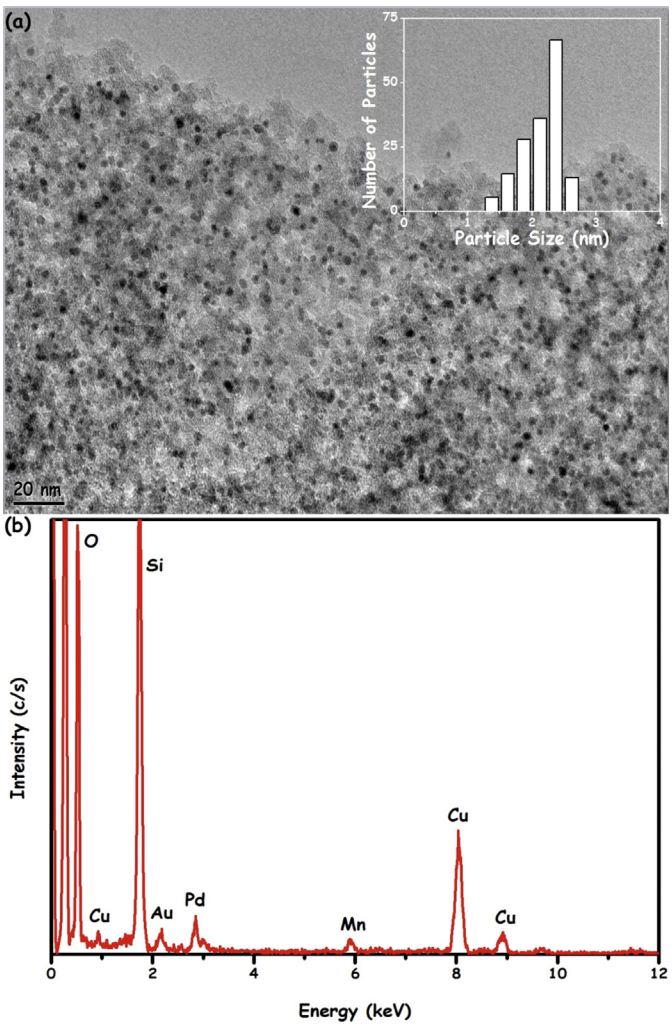

Fig. 4. (a) BFTEM image and corresponding size histogram (inset), (b) TEM-EDX spectrum of $Pd_{0.5}Au_{0.3}Mn_{0.2}$/N-SiO_2 catalyst.

Au (*i.e.*, Au^0 with Au $4f_{7/2}$ at 82.2 eV and Au $4f_{5/2}$ at 86.1 eV) [34]. On the other hand, Mn was found to exist in the form of Mn^{2+} (Mn $2p_{3/2}$ at 640.1 eV), Mn^{3+} (Mn $2p_{3/2}$ at 641.2 eV) and Mn^{4+} (Mn $2p_{3/2}$ at 642.6 eV) [35,36] exhibiting an additional high-binding energy shake-up peak feature at 645.3 eV [36]. The existence of mixed oxide states of Mn can be attributed to the high oxophilicity of Mn, which makes metallic Mn^0 highly reactive upon exposure to air leading to the formation of MnO_x states with high stability [37,38]. P-XRD patterns of PdAu-MnO_x/N-SiO_2, Pd/N-SiO_2, Au/N-SiO_2 and Mn/N-SiO_2 are given in Fig. 2. P-XRD pattern of PdAu-MnO_x/N-SiO_2 catalyst exhibits a new diffraction peak located between the characteristic Pd and Au diffraction features, indicating the formation of alloy structure [20]. In addition to that, DR-UV–vis spectrum taken from solid powders of PdAu-MnO_x/N-SiO_2 (Fig. 3) show almost no surface plasmon resonance band for Au NPs, whereas Au/N-SiO_2 have surface plasmon resonance bands at near 520 nm. This surface plasmon resonance quenching caused by alloying was also observed in oleylamine stabilized PdAu [20] and PdAg [21] alloy NPs.

BFTEM, TEM-EDX and STEM-EDX-point analyses were performed to examine the size, morphology and the composition of the PdAu-MnO_x/N-SiO_2. BFTEM image of PdAu-MnO_x/N-SiO_2 given in Fig 4(a) reveals that the presence of PdAu and MnO_x nanoparticles. The mean particle size of the resulting PdAu-MnO_x nanoparticles was found to be ca. 2.1 nm using the NIH image program [39], which included the particle size analysis for >100 non-touching particles (inset in Fig. 4(a)). EDX analysis during BFTEM observation from many different areas confirmed the presence of Pd, Au and Mn in the analyzed regions (Fig. 4(b)). STEM-EDX point analyses performed on three separated particles are presented in Fig. 5, which show the existence of separately nucleated PdAu alloy (points 1 and 2) and MnO_x (point 3) particles. These results (P-XRD, DR-UV–vis, STEM-EDX-point analyses) support the presence of individual PdAu alloy NPs that are separate from the MnO_x NPs on the N-SiO_2 support surface. On the other hand, as it is difficult to establish an accurate statistical analysis using microscopic probes, presence of a minor amount of overlapping domains of PdAu and MnO_x nanoparticles cannot be excluded.

The catalytic activities of $Pd_{0.5}Au_{0.3}Mn_{0.2}$/N-SiO_2 together with its monometallic, bimetallic and trimetallic counterparts in different molar compositions were investigated in the dehydrogenation of aqueous FA solution (0.20 M in 10.0 mL H_2O) at 298 K and their results are given in Fig. 6(a)–(c). Evidently, $Pd_{0.5}Au_{0.3}Mn_{0.2}$/N-SiO_2 catalyst provides a better activity than those of mono and bimetallic catalysts prepared by the same method. From Fig. 6(a) and (b), it is clear that Pd is the crucial active metal in all catalysts; without Pd addition $Au_{1.0}$/N-SiO_2, $Mn_{1.0}$/N-SiO_2, and $Au_{0.51}Mn_{0.49}$/N-SiO_2 catalysts show almost no activity. Although, bimetallic $Pd_{0.52}Au_{0.48}$/N-SiO_2 and $Pd_{0.55}Mn_{0.45}$/N-SiO_2 catalysts show better activities than $Pd_{1.0}$/N-SiO_2, their performances are still far inferior to the trimetallic $Pd_{0.5}Au_{0.3}Mn_{0.2}$/N-SiO_2. The enhanced catalytic activity of $Pd_{0.5}Au_{0.3}Mn_{0.2}$/N-SiO_2 can be ascribed to the combination of the surface electronic state in

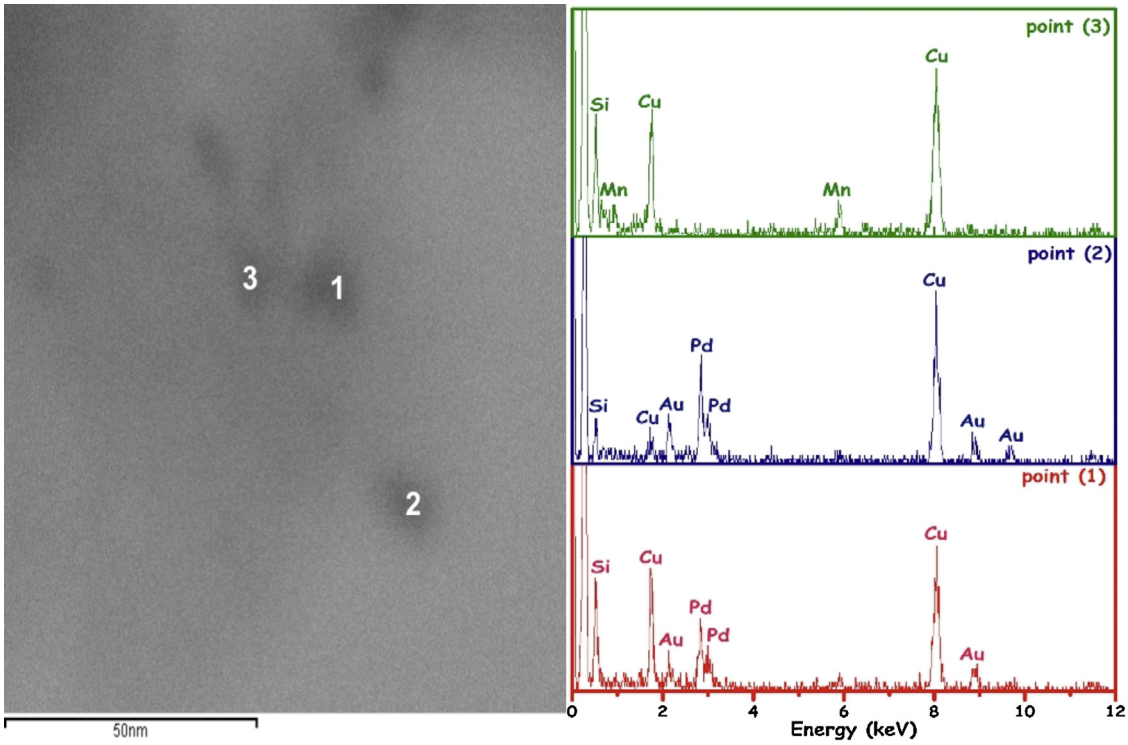

Fig. 5. STEM image and STEM-EDX spectra of $Pd_{0.5}Au_{0.3}Mn_{0.2}$/N-SiO_2 catalyst collected from three separate points given in STEM image.

PdAu alloy structure [20] and the effect of separately nucleated MnO_x nanoparticles on PdAu alloy nanoparticles [22] (*vice versa*), which was further supported by the result of a control experiment in which the physical mixture of $Pd_{0.52}$/N-SiO_2, $Au_{0.27}$/N-SiO_2 and $Mn_{0.21}$/N-SiO_2 displays lower reactivity than $Pd_{0.5}Au_{0.3}Mn_{0.2}$/N-SiO_2 catalyst in the dehydrogenation of FA under identical conditions (Fig. 6(d)). The collected gas from FA dehydrogenation over $Pd_{0.5}Au_{0.3}Mn_{0.2}$/N-SiO_2 catalyst was analyzed by gas chromatography (GC), infrared spectroscopy (FTIR) and NaOH trap experiment (Fig. S2–S4). The sum of their results revealed that the generated gas is a mixture of H_2 and CO_2 with a molar ratio of 1.0:1.0, where CO was below the detection limit (*i.e.*, <10 ppm). In other words, these experiments point to the important fact that CO-free H_2 production can be achieved from $Pd_{0.5}Au_{0.3}Mn_{0.2}$/N-SiO_2 catalyzed dehydrogenation of FA for fuel cell applications.

Fig. 7(a) shows the plot of the volume of generated gas ($H_2 + CO_2$) *versus* time for $Pd_{0.5}Au_{0.3}Mn_{0.2}$/N-SiO_2 catalyzed dehydrogenation of aqueous FA solution (0.20 M in 10.0 mL H_2O) starting with various catalyst concentrations ([PdAuMn]) at 298 K. We found that only ~3.0 mol% $Pd_{0.5}Au_{0.3}Mn_{0.2}$/N-SiO_2 ([PdAuMn] = 6.25 mM) can catalyze the room temperature FA dehydrogenation at >92% conversion with an initial TOF value of 785 mol H_2 mol catalyst^{-1} h^{-1} (details for the calculation of initial TOF value is given in the Supplementary information). To the best of our knowledge, this is the highest TOF value ever reported for FA dehydrogenation at room temperature using a heterogeneous catalyst without utilizing any additives (Table 1) and is even comparable to the most of homogeneous catalysts [5]. More importantly, FA dehydrogenation can be completed within a 5 min. at >85 % conversion measured at 298 K. The observed rate constants (k_{obs}) for each catalyst concentration were calculated from the linear portion of each plot given in Fig. 7(a) and found to be 19.2, 22.6, 34.0 and 40.0 mL gas/min for the catalyst concentration of 2.50, 3.75, 5.00 and 6.25 mM, respectively. The logarithmic plot of k_{obs} versus catalyst concentration (Fig. 7(b)) gives a line with a slope of 0.93, which is indicative of $Pd_{0.5}Au_{0.3}Mn_{0.2}$/N-SiO_2 catalyzed additive-free FA dehydrogenation, is close to first-order with respect to the catalyst concentration within the investigated concentration window. The enhancement of Pd activity in FA dehydrogenation through Au incorporation has already been reported for CoAuPd [18,19] and AuPd [20,23] NPs, in which the activity increase has been attributed to a synergic effect [40]. In this context, to shed some light on the effect of separately nucleated MnO_x NPs on the catalytic reactivity of PdAu alloy nanoparticles we conducted CO stripping voltammetry experiments over Pd/N-SiO_2, PdAu/N-SiO_2 and PdAu-MnO_x/N-SiO_2 catalysts (Figs. S5–S7). Fig. 8 gives CO-stripping voltammograms for Pd/N-SiO_2, PdAu/N-SiO_2 and PdAu-MnO_x/N-SiO_2 catalysts. The onset potential of CO oxidation on PdAu-MnO_x/N-SiO_2 (0.52 V) is lower than those of Pd/N-SiO_2 (0.67 V) and PdAu/N-SiO_2 (0.68 V).

Table 1
Comparison of the catalytic performance data for the currently studied PdAu-MnO_x/SiO_2-NH2 catalyst with the prior best heterogeneous catalyst systems reported for the dehydrogenation FA in the absence of any additives at low temperatures.

Catalyst	Temp. (K)	Con. (%)	Activity[a]	Reference
Ag@Pd	293	36	63	[16]
AgPd	293	10	72	[16]
Ag@Pd/C	293	44	96	[16]
Au@Pd/N-rGO	298	89	98	[17]
CoAuPd/C	298	91	37	[18]
CoAuPd/r-GO	298	51	45	[19]
CoAuPd/DNA	298	96	85	[19]
AuPd	298	28	41	[20]
AgPd	298	52	150	[21]
Pd-MnO_x/N-SiO_2	293	80	140	[22]
PdAu-MnO_x/Graphene-ZIF-8[b]	298	94	382	[23]
PdAu-MnO_x/Graphene-ZIF-8[c]	298	94	180	[23]
Pd-MnO_x/Graphene-ZIF-8	298	60	136	[23]
PdAu-MnO_x/N-SiO_2[c]	298	92	785	This study

[a] TOF = mol H_2/mol catalyst × time (h).
[b] TOF value was calculated based on Au and Pd atoms.
[c] TOF value was calculated based on Au, Pd and Mn atoms.

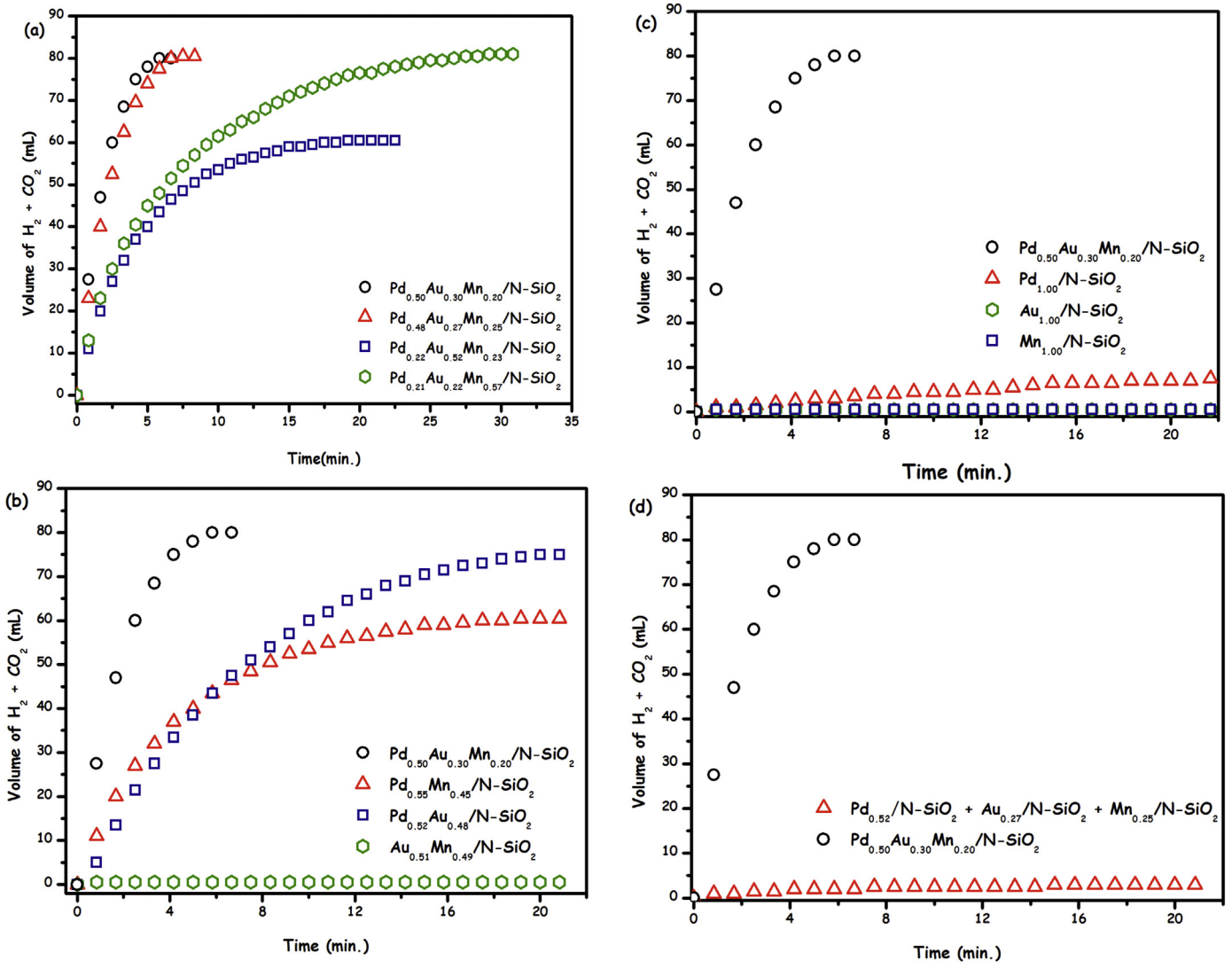

Fig. 6. The volume of generated gas ($H_2 + CO_2$) (mL) versus time (min) graphs of (a) monometallic, (b) bimetallic, (c) trimetallic catalysts in the additive-free dehydrogenation of FA (0.20 M in 10.0 mL H_2O) starting with identical catalyst concentrations at 298 K, (d) the volume of generated gas ($H_2 + CO_2$) (mL) versus time (min) graph for the additive-free dehydrogenation of FA (0.20 M in 10.0 mL H_2O) in the presence of $Pd_{0.5}Au_{0.3}Mn_{0.2}$/N-SiO_2 catalyst or the physical mixture of $Pd_{0.52}$/N-SiO_2, $Au_{0.27}$/N-SiO_2 and $Mn_{0.21}$/N-SiO_2 catalysts at 298 K.

This observation suggests that the existence of separately nucleated MnO_x facilitates the removal of CO from the surface of active PdAu nanoparticles. This experiment clearly demonstrates that the CO poisoning resistance of PdAu alloy nanoparticles can be significantly enhanced by the promotional effect of MnO_x NPs.

Then, to understand the effect of surface grafted amine group on the catalytic reactivity of PdAu-MnO_x nanoparticles, we conducted two control experiments, in which the activity of metal free amine-grafted SiO_2 and PdAu-MnO_x nanoparticles supported on amine-free SiO_2 were investigated in the FA dehydrogenation under identical conditions. We found that metal free amine-grafted SiO_2 is catalytically inactive and amine-free SiO_2 supported PdAu-MnO_x catalyst ($Pd_{0.49}Au_{0.32}Mn_{0.19}/SiO_2$) provides lower catalytic performance (initial TOF = 130 mol H_2 mol catalyst^{-1} h^{-1} and 54% conversion) than that of $Pd_{0.5}Au_{0.3}Mn_{0.2}$/N-SiO_2 (Fig. 9(a)). The lower reactivity of $Pd_{0.49}Au_{0.32}Mn_{0.19}/SiO_2$ can be explained by the absence of $-NH_2$ functionalities on the support material, which may have a direct impact on the FA adsorption/storage process as well as the nucleation and growth of the PdAu-MnO_x nanoparticles on the support surface. BFTEM image of $Pd_{0.49}Au_{0.32}Mn_{0.19}/SiO_2$ catalyst given in Fig. 9(b) reveals that the existence of highly clumped particles (*d*mean = 7.5 nm inset of Fig. 9(b)) with respect to $Pd_{0.5}Au_{0.3}Mn_{0.2}$/N-SiO_2, which demonstrates the stabilizing effect of surface grafted amine groups [41,42]. Additionally, the recent mechanistic study conducting for the amine assisted PdAg catalyzed FA dehydrogenation [27] has already showed that that O—H bond cleavage is facilitated with the assistance of $-N(CH_3)_2$ group and leads to the formation of metal-formate species along with a $-[N(CH_3)_2H]^+$ group, which, then, undergo further dehydrogenation to produce H_2 and CO_2. In the light of these results, it is logical to comprehend that the surface grafted amine groups of APTS in our support acts as a proton forager and provides a basic environment around PdAu-MnO_x nanoparticles, which profits the O—H bond dissociation that is subsequently linked with the C—H bond cleavage from the metal-formate intermediate to release H_2.

Fig. 10(a) shows the plot of the volume of generated gas ($H_2 + CO_2$) *versus* time for $Pd_{0.5}Au_{0.3}Mn_{0.2}$/N-SiO_2 catalyzed dehydrogenation of aqueous FA solution (0.20 M in 10.0 mL H_2O) at different temperatures (298, 308, 318 and 328 K). Expectedly, the activity of $Pd_{0.5}Au_{0.3}Mn_{0.2}$/N-SiO_2 catalyst enhances by the increase of the temperature. The observed rate constants were found to be 19.0, 25.0, 37.5, and 49.0 mL gas min^{-1} at 298, 308, 318

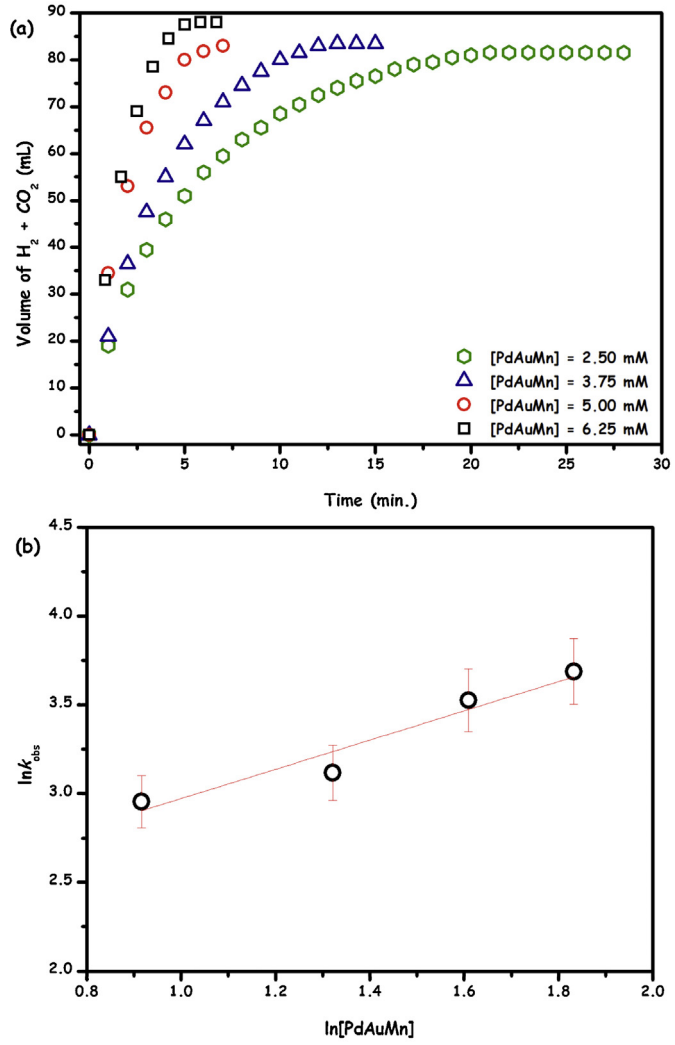

Fig. 7. (a) The volume of generated gas (H_2 + CO_2) (mL) versus time (min) graphs for $Pd_{0.5}Au_{0.3}Mn_{0.2}$/N-SiO_2 catalyzed additive-free dehydrogenation of FA (0.20 M in 10.0 mL H_2O) at 298 K starting with various catalyst concentrations [PdAuMn], (b) the corresponding observed rate constants versus catalyst concentrations (both in logarithmic scales) graph.

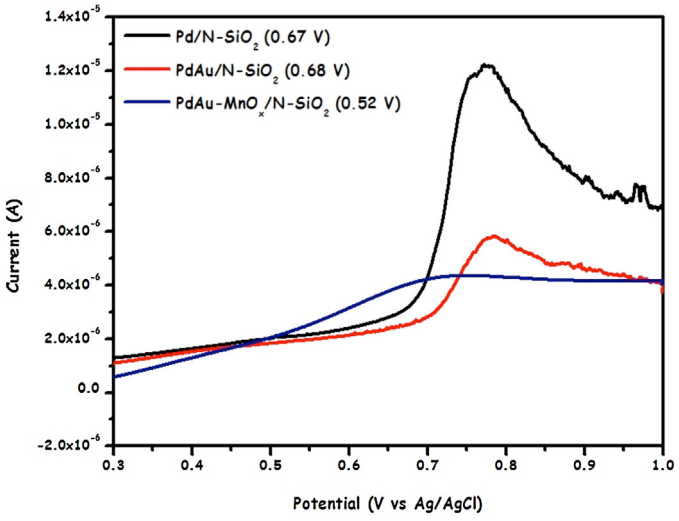

Fig. 8. CO-stripping voltamograms (for clarity only forward scans are given) for Pd/N-SiO_2, PdAu/N-SiO_2 and PdAu-MnO_x/N-SiO_2 catalysts in H_2SO_4 solution at 10 mV s^{-1} scan rate.

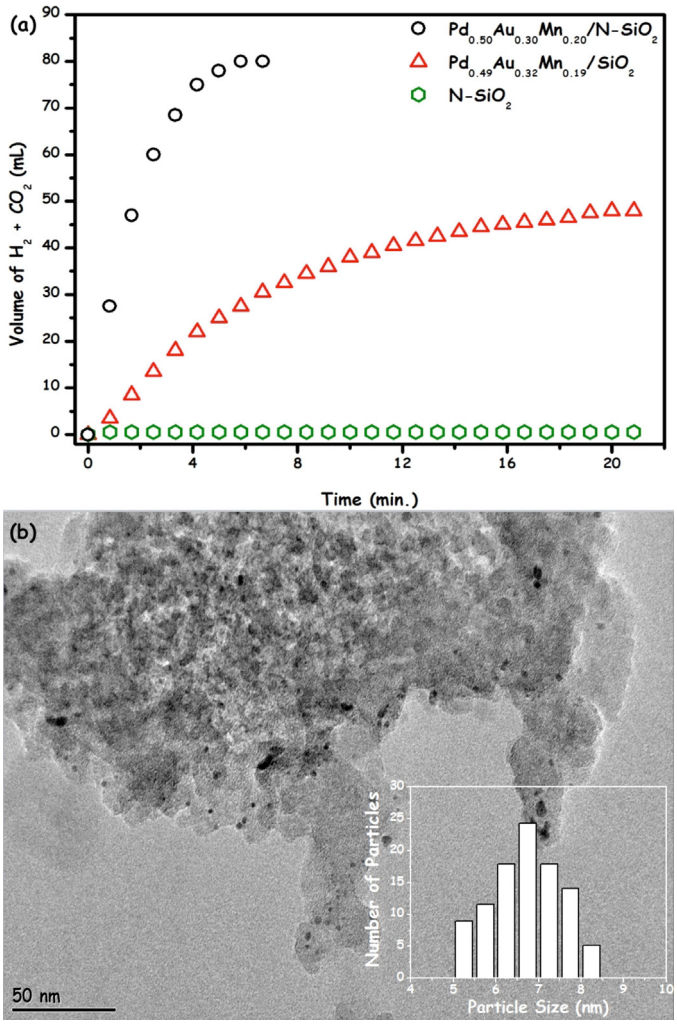

Fig. 9. (a) The volume of generated gas (H_2 + CO_2) (mL) versus time (min) graphs for the additive-free dehydrogenation of FA (0.20 M in 10.0 mL H_2O) at 298 K in the presence of $Pd_{0.5}Au_{0.3}Mn_{0.2}$/N-SiO_2, $Pd_{0.49}Au_{0.32}Mn_{0.19}$/$SiO_2$ catalysts and N-SiO_2 support, (b) BFTEM image and corresponding size histogram (inset) of $Pd_{0.49}Au_{0.32}Mn_{0.19}$/$SiO_2$ catalyst.

and 328 K, respectively. These observed rate constants (k_{obs}) at four different temperatures were used to obtain Arrhenius and Eyring plots (Fig. 10(b)–(c)) to calculate activation parameters. Using these plots, activation energy (E_a), activation enthalpy ($\Delta H^{\neq}$) and activation entropy ($\Delta S^{\neq}$) values were calculated to be 26.2 kJ/mol, 23.8 kJ/mol and −140 J/mol.K, respectively. Assuming that the activation parameters calculated from the macroscopic kinetic data given above are relevant to the most critical activation step in the FA dehydrogenation mechanism, one can argue that the positive magnitude of the apparent activation enthalpy and the large negative value of apparent activation entropy imply the presence of a associative mechanism at the transition state [43].

The catalytic durability of $Pd_{0.5}Au_{0.3}Mn_{0.2}$/N-SiO_2 catalyst in FA dehydrogenation was investigated by performing reusability experiments. After the complete dehydrogenation of FA, $Pd_{0.5}Au_{0.3}Mn_{0.2}$/N-SiO_2 catalyst was isolated as a dark gray powder and bottled under nitrogen atmosphere. Then, the isolated $Pd_{0.5}Au_{0.3}Mn_{0.2}$/N-SiO_2 catalyst was re-dispersed in the aqueous FA solution. This re-dispersed catalyst preserved 92% of its initial activity with a 85% conversion of FA to CO_2 and H_2 even after the 5th catalytic reuse (Fig. 11(a)). The elemental composition, crystallinity and morphological analyses of reused $Pd_{0.5}Au_{0.3}Mn_{0.2}$/N-SiO_2 catalyst were done by BFTEM, P-XRD, ICP-OES analyses and ninhydrin

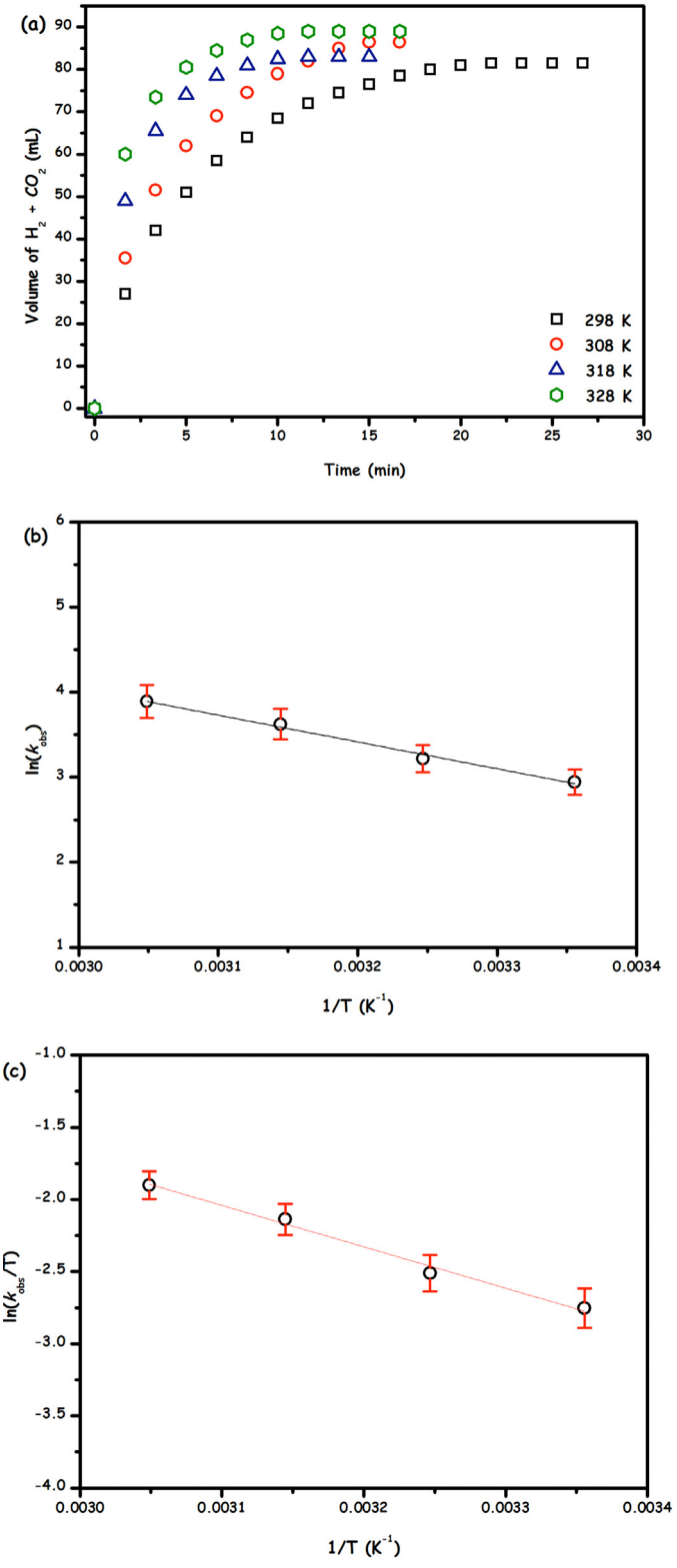

Fig. 10. (a) The volume of generated gas (H_2 + CO_2) (mL) versus time (min) graphs for $Pd_{0.5}Au_{0.3}Mn_{0.2}$/N-SiO_2 catalyzed (2.50 mM) additive-free dehydrogenation of FA (0.20 M in 10.0 mL H_2O) at different temperatures, (b) Arrhenius ($y = 13.51 - 3154x$; $R^2 = 0.987$) and (c) Eyring plots ($y = 6.85 - 2868x$; $R^2 = 0.989$).

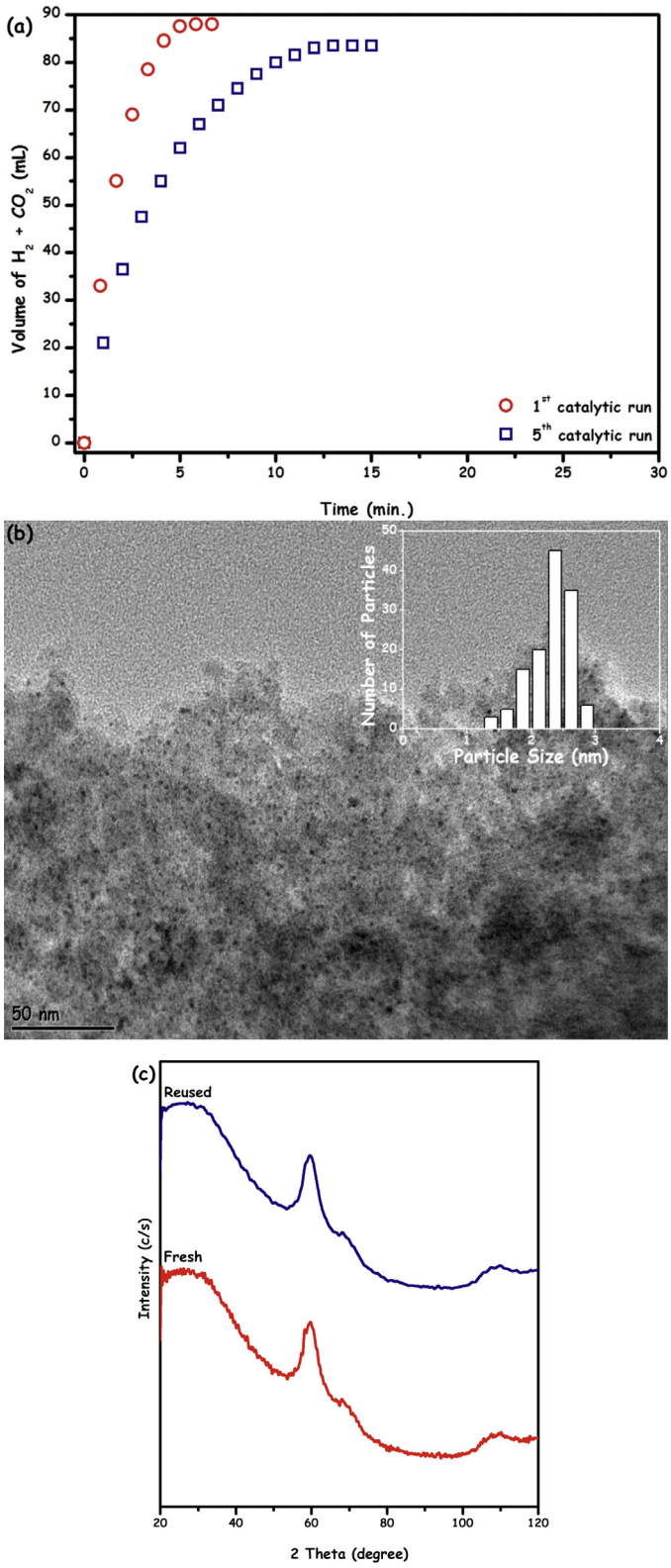

Fig. 11. (a) The volume of generated gas (H_2 + CO_2) (mL) versus time (min) graphs obtained from the 1st and 5th catalytic runs for the dehydrogenation of aqueous FA catalyzed by $Pd_{0.5}Au_{0.3}Mn_{0.2}$/N-SiO_2 at 298 K, (b) representative BFTEM image of P $Pd_{0.5}Au_{0.3}Mn_{0.2}$/N-SiO_2 catalyst harvested after 5th catalytic reuse, (c) P-XRD patterns of fresh and reused $Pd_{0.5}Au_{0.3}Mn_{0.2}$/N-SiO_2 catalysts.

method. Fig. 11(b) shows the BFTEM image $Pd_{0.5}Au_{0.3}Mn_{0.2}$/N-SiO_2 catalyst harvested after 5th catalytic reuse. The size analyses of the resulting PdAu-MnO_x nanoparticles (inset in Fig. 11(b)) indicative of a small increase in the average size of the reused nanoparticles throughout the reusability experiments from 2.2 nm (fresh) to 2.8 nm (after 5th reuse), which explains the slight decrease in the observed activity of $Pd_{0.5}Au_{0.3}Mn_{0.2}$/N-SiO_2 catalyst. The comparison of P-XRD patterns of fresh and reused catalyst (Fig. 11(c)) shows that the crystallinity of the fresh and reused catalysts is identical. ICP-OES and elemental analyses of the recovered $Pd_{0.5}Au_{0.3}Mn_{0.2}$/N-SiO_2 catalyst gave us almost the identical Pd, Au, Mn and $-NH_2$ loading amounts with that of the fresh catalyst. Additionally, the catalytic dehydrogenation of FA was completely stopped by the removal of $Pd_{0.5}Au_{0.3}Mn_{0.2}$/N-SiO_2 catalyst from the reaction solution; these results confirm no leaching of active metal nanoparticles into the solution.

4. Conclusions

In summary, PdAu-MnO_x/N-SiO_2 catalyst was prepared, for the first time, by using a simple and reproducible procedure. The characterization of this new catalytic material was done by a combination of complimentary techniques, which revealed that the formation of well-dispersed separately nucleated PdAu alloy and MnO_x nanoparticles with an average diameter of 2.2 nm supported on APTS functionalized SiO_2 support. The catalytic employment of PdAu-MnO_x/N-SiO_2 catalyst was demonstrated in the additive-free dehydrogenation of FA, in which it provides a record-high activity (860 mol H_2 mol catalyst^{-1} h^{-1}) and excellent conversion (>92%) converging to that of the existing state of the art homogenous catalytic systems available for FA dehydrogenation in the absence of additives. Moreover, it shows high stability against to leaching and agglomeration that makes it highly reusable catalyst (>92 % activity and 85% conversion even at 5th run) in the additive-free FA dehydrogenation. This uniquely active, selective and stable catalyst has a strong potential to be exploited in practical/technological applications, where FA is utilized as a viable hydrogen carrier in mobile fuel cell applications.

Acknowledgements

MZ thanks to Yüzüncü Yıl University Office of Scientific Research Projects for the financial support to his research laboratory. Additionally, the partial supports by Fevzi Akkaya Scientific Activities Support Fund (FABED), Science Academy and Turkish Academy of Sciences (TUBA) are gratefully acknowledged.

Appendix A. Supplementary data

Supplementary data associated with this article can be found, in the online version, at http://dx.doi.org/10.1016/j.apcatb.2015.06.060

References

[1] J. Graetz, Chem. Soc. Rev. 38 (2009) 73–82.
[2] N.Z. Muradova, T.N. Veziroglu, Int J. Hydrog. Energy 30 (2005) 225–237.
[3] J.A. Turner, Science 285 (1999) 687–689.
[4] L. Schlaphach, A. Zuttel, Nature 414 (2001) 353–358.
[5] S. Enthaler, J.V. Langermann, T. Schmidt, Energy Environ. Sci. 3 (2010) 1207.
[6] M. Yadav, Q. Xu, Energy Environ. Sci. 5 (2012) 9698.
[7] K.V. Kordesch, G.R. Simader, Chem. Rev. 95 (1995) 191.
[8] T.C. Johnson, D.J. Morris, M. Wills, Chem. Soc. Rev. 39 (2010) 81.
[9] M. Grasemann, G. Laurenzcy, Energy Environ. Sci. 5 (2012) 8171.
[10] S. Fukuzimi, T. Kobayashi, T. Suenobu, J. Am. Chem. Soc. 132 (2010) 1496.
[11] A. Boddien, D. Mellmann, F. Gaertner, R. Jackstell, H. Junge, P.J. Dyson, G. Laurenczy, R. Ludwig, M. Beller, Science 333 (2011) 1733.
[12] J.D. Scholten, M.H.G. Prechtl, J. Dupont, ChemCatChem 2 (2010) 1265.
[13] Q.L. Zhu, N. Tsumori, Q. Xu, Chem. Sci. 5 (2014) 195.
[14] X. Zhou, Y. Huang, W. Xing, C. Liu, J. Liao, T. Lu, Chem. Commun. (2008) 3540.
[15] Q.Y. Bi, X.L. Du, Y.M. Liu, Y. Cao, H.Y. He, K.N. Fan, J. Am. Chem. Soc. 134 (2012) 8926.
[16] K. Tedsree, T. Li, S. Jones, C.W.A. Chan, K.M.K. Yu, P.A.J. Bagot, E.A. Marquis, G.D.W. Smith, S.C.E. Tsang, Nat. Nanotech. 6 (2011) 302.
[17] Z.L. Wang, J.M. Yan, H.L. Wang, Y. Ping, Q. Jiang, J. Mater. Chem. A 1 (2013) 12721.
[18] Z.L. Wang, J.M. Yan, Y. Ping, H.L. Wang, W.T. Zheng, Q. Jiang, Angew. Chem. Int. Ed. 52 (2013) 4406.
[19] Z.L. Wang, H.L. Wang, J.M. Yan, Y. Ping, S.J. Li, Q. Jiang, Chem. Commun. 50 (2014) 2732.
[20] Ö. Metin, X. Sun, S. Sun, Nanoscale 5 (2013) 910.
[21] H. Zhang, Ö. Metin, D. Su, S. Sun, Angew. Chem. Int. Ed. 52 (2013) 3681.
[22] A. Bulut, M. Yurderi, Y. Karatas, M. Zahmakiran, H. Kivrak, M. Gulcan, M. Kaya, Appl. Cat. B: Environ. 164 (2015) 324.
[23] J.-M. Yan, Z.-L. Wang, L. Gu, S.-J. Li, H.-L. Wang, W.-T. Zheng, Q. Jiang, Adv. Energy Mater. (2015) 1500107.
[24] X. Gu, Z.-H. Lu, H.-L. Jiang, T. Akita, Q.J. Xu, Am. Chem. Soc. 133 (2011) 11822.
[25] B. Loges, A. Boddien, H. Jınge, M. Beller, Angew. Chem. Int. Ed. 47 (2008) 3962.
[26] E.A. Bielinski, P.O. Lagaditis, Y. Zhang, B.Q. Mercado, C. Würtele, W.H. Bernskoetter, N. Hazari, S. Schneider, J. Am. Chem. Soc. 136 (2014) 10234.
[27] K. Mori, M. Dojo, H. Yamashita, ACS Catal. 3 (2013) 1114.
[28] M. Yadav, T. Akita, N. Tsumori, Q. Xu, J. Mater. Chem. 22 (2012) 12582.
[29] M. Yurderi, A. Bulut, M. Zahmakiran, M. Kaya, App. Catal. B: Environ. 160 (2014) 514.
[30] I. Taylor, A.G. Howard, Anal. Chim. Acta 271 (1993) 77.
[31] R.J. White, R. Luque, V.L. Budarin, J.H. Clark, D.J. Macquarrie, Chem. Soc. Rev. 38 (2009) 481.
[32] C. Perreira, J.F. Silva, A.M. Perreira, J.P. Araujo, G. Blanco, J.M. Pintado, C. Freire, Catal. Sci. Technol. 1 (2011) 784.
[33] Y. Zhang, J. Ouyang, H. Yang, Sci. Rep. 3 (2013) 1.
[34] Y. Shi, J.-K. Huang, L. Jin, Y.-T. Hsu, S.F. Yu, L.-J. Li, H.Y. Yang, Sci. Rep. 3 (2013) 1839.
[35] M. Kang, E.D. Park, J.M. Kim, J.E. Yie, Appl. Catal. A: Genet. 327 (2007) 261.
[36] X. Wang, Q. Kang, D. Li, Appl. Catal. B: Environ. 86 (2009) 166.
[37] J.F. Bondi, K.D. Oyler, X. Ke, P. Schiffer, R.E. Schaak, J. Am. Chem. Soc. 131 (2009) 9144.
[38] P.Z. Si, E. Brueck, Z.D. Zhang, O. Tegus, W.S. Zhang, K.H.J. Buschow, J.C.P. Klaasse, Mater. Res. Bull. 40 (2005) 29.
[39] J.E. Hutchison, G.H. Woehrie, S. Özkar, R.G. Finke, Turkish J. Chem. 30 (2006) 1.
[40] J.S. Yoo, F.A. Pedersen, J.K. Norskov, F. Studt, ACS Catal. 4 (2014) 1226.
[41] M. Zahmakiran, M. Tristany, K. Philippot, S. Özkar, B. Chaudret, Dalton Trans. 41 (2012) 590.
[42] M. Zahmakiran, M. Tristany, K. Philippot, K. Fajerwerg, S. Özkar, B. Chaudret, Chem. Commun. 46 (2010) 2938.
[43] K.A. Connors, Theory of Chemical Kinetics, VCH Publishers, New York, 1990.